Focusing Technique for Holographic Subsurface Radar Based on Image Entropy

Haewon Jung*, Dal-Jae Yun, and Hoon Kang

Advanced Instrumentation Institute
Korea Research Institute of Standards and Science, Daejeon, 34113, Republic of Korea
*haewon.jung@kriss.re.kr, daljae.yun@kriss.re.kr, hkang@kriss.re.kr

Abstract ─ An image focusing method for holographic subsurface radar (HSR) is proposed herein. HSR is increasingly being utilized to survey objects buried at shallow depths and the acquired signals are converted into an image by a reconstruction algorithm. However, that algorithm requires actual depth and material information or depends on human decisions. In this paper, an entropy-based image focusing technique is proposed and validated by numerical simulation software package based on finite-difference time-domain method and experiment. The resulting images show good agreement with the actual positions and shapes of the targets.

Index Terms ─ Autofocusing, entropy, holographic subsurface radar, image reconstruction.

I. INTRODUCTION

Subsurface radar techniques are being widely used to image and identify concealed structures and objects. Typically for these tasks, two types of subsurface radar techniques are used: ground penetrating radar (GPR) and holographic subsurface radar (HSR) [1, 2].

The GPR technique is commonly utilized to investigate subsurface regions using impulse or ultra-wideband signals, because these signals can effectively penetrate subsurface materials. However, in a shallow region, reconstructed GPR images suffer from ghost images caused by multiple reflections. For these reasons, the HSR technique is increasingly being applied for subsurface imaging in shallow regions. This is due to its features of high resolution and freedom from multiple reflections between radiator and target, or from the target itself [3, 4].

Recently, the HSR technique has been actively researched for detection and imaging of subsurface objects such as defects in insulation forms, landmines, building structures, and weapons [5–9]. With HSR, the radar image is gathered at a plane located above the plane of the object of interest. Due to the gap between the measuring and object plane, which is filled with air or dielectric material, a raw image resulting from the survey on the measuring plane can be reconstructed using the proper algorithms [3, 5].

For proper algorithm processing, the depth of the object plane and relative permittivity (RP) of the subsurface materials are required to obtain a clear image. However, the RP may not be known exactly in a survey environment, so whether the radar image is clear and well-focused is judged by the operator. In this paper, we apply an entropy-based image focusing method to reconstruct automatically an HSR image when subsurface materials and depth of the target are unknown.

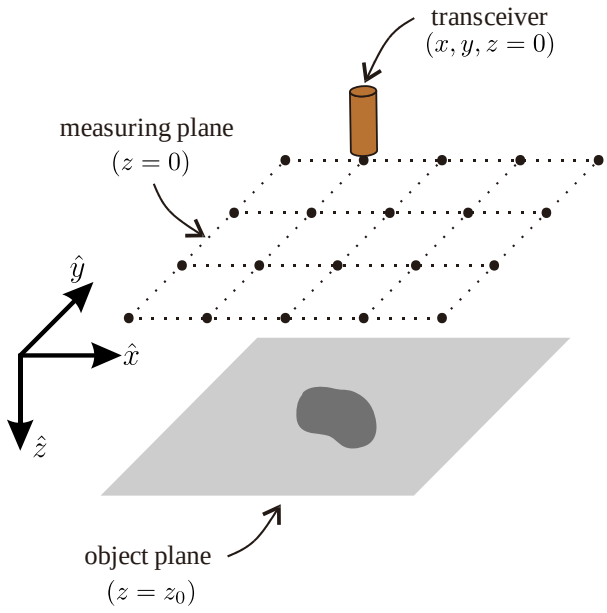

Fig. 1. Geometry for HSR image data acquisition model.

II. HOLOGRAPHIC SUBSURFACE RADAR IMAGING

The HSR technique configures a subsurface region as a plan-view image, which originated as an optical holography technique proposed by Gabor [10]. Details of the HSR principles and equations are described in recent research [1–8].

Submitted On: October 26, 2020
Accepted On: March 14, 2021
https://doi.org/10.47037/2020.ACES.J.360402

The method calls for acquisition of raw data in a two-dimensional (2D) geometry that can be modelled as shown in Fig. 1. The transceiver, typically an open-end waveguide with rectangular or circular shape, surveys the measuring plane in uniform sweeps in the *x* and *y* directions.

The raw image produced directly from the raw data has a look similar to that of the actual objects because the electromagnetic wave propagating through the open-end waveguide is highly attenuated outside of the waveguide [3]. Nevertheless, the raw data can be focused to provide a clear image using the reconstruction algorithms.

The raw data is composed of complex amplitudes depending on the *x* and *y* position; and they should be obtained at single or multiple frequency points. Then the raw data can be represented as $u(x, y, z = 0)$ and $u(x, y, z = 0, \omega)$ at a single and multiple frequency points respectively, where $x = x_1, x_2, \dots, x_m$ and $y = y_1, y_2, \dots, y_n$ positions, and $\omega = \omega_1, \omega_2, \dots, \omega_p$. The spatial sampling intervals Δx and Δy must be less than quarter wavelength to satisfy the Nyquist criterion [2]. Then the spectral sampling intervals can be defined by the spatial ones.

In the case of a single frequency, the raw data can be reconstructed as image $p(x, y, z = z_0)$ using equation (1), as follows:

$$p(x, y, z = z_0) = \mathrm{FFT}_{2D}^{-1}\begin{bmatrix}\mathrm{FFT}_{2D}[u(x, y, z = 0)] \\ \times\, e^{jk_z z_0}\end{bmatrix}. \quad (1)$$

In the multiple frequency case, the raw data $u(x, y, z = 0, \omega)$ can be reconstructed as image $p(x, y, z)$ using equation (2), as follows:

$$p(x, y, z) = \mathrm{FFT}_{3D}^{-1}\begin{bmatrix}\mathrm{FFT}_{2D}[u(x, y, z = 0, \omega)] \\ \times\, e^{jk_z z}\end{bmatrix}, \quad (2)$$

where k_z is defined from dispersion relations taking into account backward wave propagation, as shown in equation (3) [3, 8]:

$$k_z = \sqrt{4k^2 - k_x^2 - k_y^2} = \sqrt{4\left(\omega\sqrt{\varepsilon}/c\right)^2 - k_x^2 - k_y^2}. \quad (3)$$

Note that, in the multiple frequency reconstruction, the k_z vector should be interpolated to the uniform space to use the fast Fourier transform technique [6].

In equations (1–3), the variables affecting the focused image quality are the depth and material RP. Typically, to find the best focused image, a reconstruction algorithm is iteratively applied while a person checks the image quality while varying the depth and RP.

III. ENTROPY BASED HSR IMAGE FOCUSING METHOD

Autofocus is an essential technique for image-based systems. In particular, a passive autofocus system assessing an image by itself employs many kinds of image evaluation metrics. Among them, entropy is a commonly used metric that includes optical imaging, synthetic aperture radar imaging, and microscopy imaging [11–16]. When an image is represented in 2D space as $u(x_i, y_j)$, where, i = 1, 2, ..., m and j = 1, 2, ..., n, the image entropy can be obtained as follows:

$$\mathrm{E} = -\sum_{i=1}^{m}\sum_{j=1}^{n}\alpha(x_i, y_j)\ln\left[\alpha(x_i, y_j)\right], \quad (4)$$

where $\alpha(x_i, y_j) = \frac{|u(x_i, y_j)|^2}{\sum_{i=1}^{m}\sum_{j=1}^{n}|u(x_i, y_j)|}$.

Entropy based HSR reconstruction algorithm:

for all points (ω, z) {
  compute $\mathrm{E}(\omega, z)$ *using* (1) *and* (4)
}
for all ω {
  compute $\mathrm{E}_{\mathrm{diff}}(\omega)$
}
find optimum angular frequency ω_o *from* $\mathrm{E}_{\mathrm{diff}}(\omega)$
find optimum depth z_o *from* $\mathrm{E}(\omega = \omega_o, z)$

image reconstruction using ω_o, z_o, *and* (1) *or* (2)

Fig. 2. Summary of the entropy based HSR reconstruction algorithm.

In this paper, we iteratively applied an entropy metric to the HSR reconstruction algorithm. When we assumed the RP was a free space, we could adjust the image using only the depth values. For single frequency data, entropy values were evaluated as $\mathrm{E}(z)$ within $z = 0, \Delta z, 2\Delta z, \dots, N\Delta z$. Then, the depth value representing maximum entropy was selected as the optimum value. Note that the entirely evaluated entropy values were stored in the $\mathrm{E}(z)$ along the depth increments. Therefore, the optimum value can be selected from whole values regardless of the local optimums may exist.

Compared with single frequency data, multiple frequency data have the advantage of a greater amount of information. In this case, the same process used with the single frequency data was repeated for all the angular frequencies. The resulting entropy values form a 2D matrix $\mathrm{E}(\omega, z)$. In this matrix, the optimal frequency and depth can be obtained by the following procedures. Firstly, differences between the maximum and minimum entropy were calculated for all the angular frequency values, and represented as $\mathrm{E}_{\mathrm{diff}}(\omega)$. Then, the angular frequency value ω_c of the maximum difference among all the differences calculated for each frequency could be chosen and the remainder of the process was identical to that for single frequency data. The entropy-based HSR reconstruction algorithm can be summarized as in Fig. 2.

Since the penetrating depth of the HSR is typically one to two wavelength, the proposed method also can be applied in the range [2, 8]. Moreover, computational complexity of the proposed method may be represented as $O(kMN\log(MN))$ when assuming image pixels as $N \times M$ and depth intervals as k.

IV. NUMERICAL AND EXPERIMENTAL VALIDATIONS

A. Numerical validation

The proposed method was validated by numerically surveyed data. The data was produced using a gprMax software package that is based on the finite difference time domain (FDTD) method [17]. Because of the gprMax offers CUDA based graphical processing unit operation, that is proper to gather 2D geometrical data in an efficient manner [18].

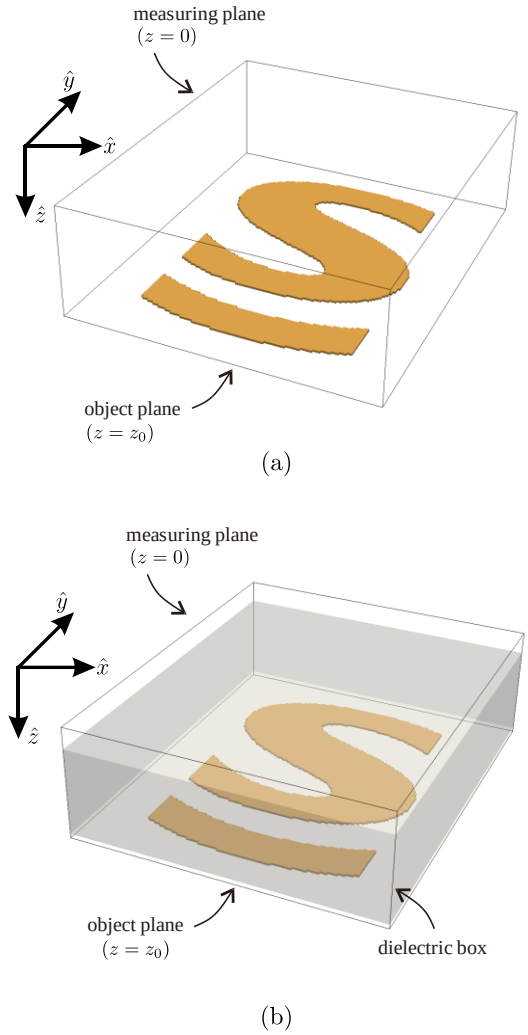

Fig. 3. Geometries for numerical validation: (a) only copper sheet target placed below the array, and (b) dielectric box placed above the copper sheet target.

In the validation, two geometries were surveyed using a copper sheet target with a special shape of letter 'S' as illustrated in Fig. 3. One is only target placing 5 cm below the surveyed array and another is dielectric box was covered with the target, where the box was composed by four RP material with 4 cm thickness. The surveyed array covers from -9 cm to +9 cm with 0.2 cm increment both in *x* and *y* directions configuring 91 × 91 array. The numerical geometry was modeled as 400 × 400 × 140 cells with 5 mm steps in *x*, *y*, and *z* directions. In the model, 1040 iterations were performed with 0.963 ns time step. And a differentiated Gaussian source with 20 GHz peak frequency was used as a point source for each acquisition of the array.

The numerically obtained data can be represented as raw images at an acquisition plane as represented in Figs. 4 (a) and (c), and reconstructed images at an object plane using the proposed method as represented in Figs. 4 (b) and (d). In the reconstruction process, the depth increments were arranged from 0 to 10 cm with 0.01 cm steps.

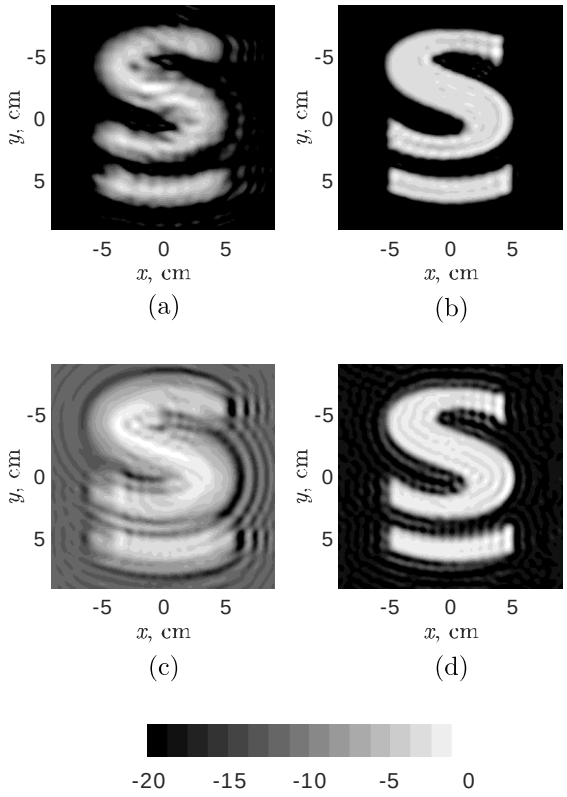

Fig. 4. Raw and reconstructed images using the proposed method via numerically obtained data: (a) raw image of target only geometry at 19.76 GHz, (b) reconstructed image of target only geometry, (c) raw image of target with dielectric box geometry at 20.49, and (d) reconstructed image of target with dielectric box geometry.

Table 1: Calculated optimal frequency and depth values of numerical validation

Target	f_o (GHz)	z_o (cm)
Free space	19.76	5.03
With dielectric box	20.49	2.59

Calculated results of optimal frequency and depth values are represented in Table 1. Compared to the raw and reconstructed images, the focused images are matched with the actual shape and position. Note that the second geometry case, optimal depth is decreased by effect of the dielectric box between surveying array and target.

B. Experimental validation

The proposed method was validated experimentally. A monostatic HSR system was made that included a vector network analyzer, three-dimensional position scanner, and a rectangular waveguide with open-end shape. The survey frequency range was from 18.5 to 19.5 GHz with 10 MHz steps. Two experiments were conducted by scanning letters with 'S' and 'ST' shapes made of silicon 2 cm thick, as shown in Fig. 5.

In the first experiment, the letter 'S' was placed 1.5 cm below the open-end of the waveguide. The scanning range was from -15 to +15 cm with steps of 0.5 cm in both the x and y directions. In the second, experiment, 'S' and 'T' were placed 6.5 and 3.5 cm below the waveguide, respectively. The scanning ranges were -35 to +35 cm and -20 to +20 cm, with 0.5 cm steps in the x and y directions, respectively.

The raw images and images reconstructed using the proposed focus method, are shown in Figs. 6 and 7. In the reconstruction process, the depth increments were arranged from 0 to 8 cm with 0.01 cm steps. The calculated entropies according to the depth increment are represented in Fig. 8. In Figs. 6 (a), 7 (a), and 7 (c), the raw images are illustrated at a single frequency calculated in the reconstruction process. In the first experiment, the optimal depth and frequency for a single target was obtained and the images were reconstructed using the depth value at single and multiple frequencies. In the second experiment, the letters were placed at different depths. Thus, the focus process was applied twice for each letter 'S' and 'T'. The results from calculation of the optimal frequency and depth values are represented in Table 2. In the table, the depth values are matched to the actual depth of the target. Compared to the raw images, each reconstructed image of a letter shows fewer layers in the shape. This reduction of the layering leads to better focused images with increased sharpness. This shows that the proposed method works well for automated focusing of HSR images.

Table 2: Calculated optimal frequency and depth values of experimental validation

Target	f_o (GHz)	z_o (cm)
'S' only	18.81	1.53
'S' of 'ST'	19.29	6.89
'T' of 'ST'	18.56	3.58

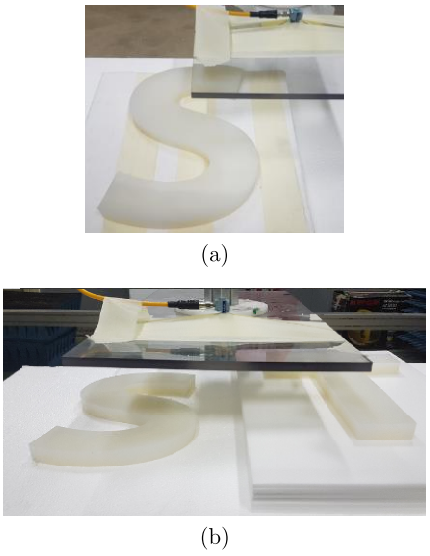

Fig. 5. Experimental setup for measuring letter 'S' and letters 'ST'.

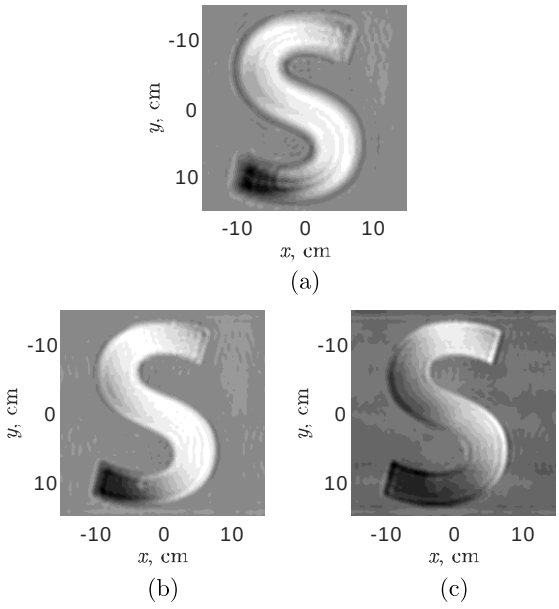

Fig. 6. Raw and reconstructed images using the proposed method: (a) raw image of letter 'S' at 18.81 GHz, (b) reconstructed image of 'S' at 18.81 GHz, and (c) reconstructed image of letter 'S' at multiple frequencies.

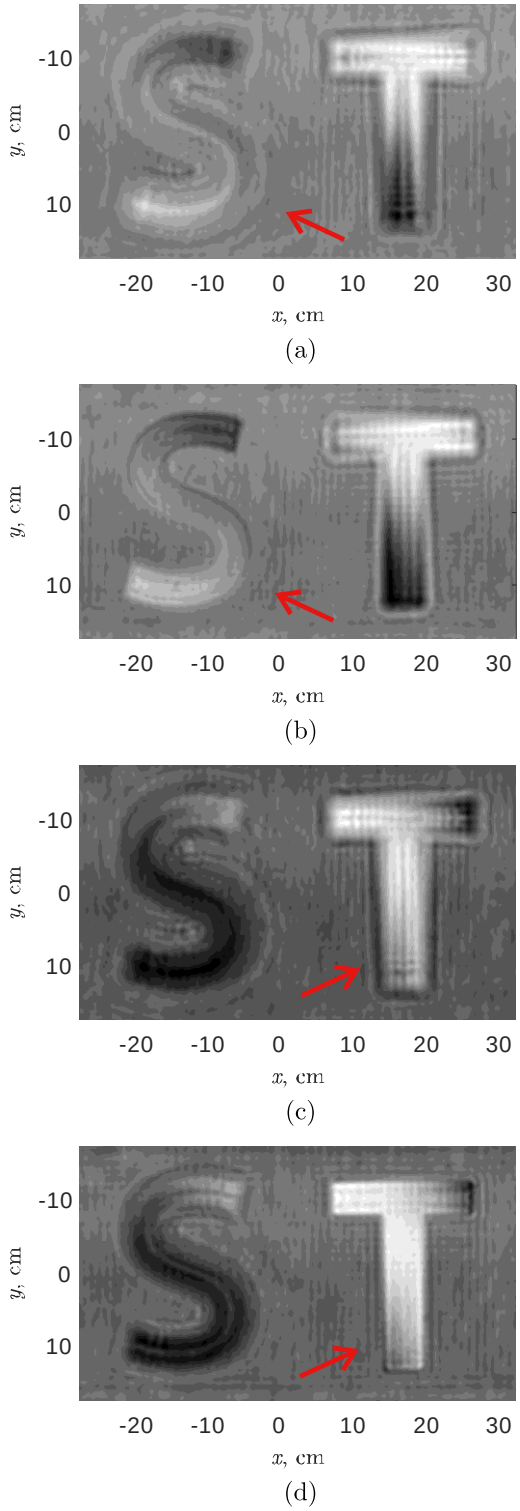

Fig. 7. Raw and reconstructed images using the proposed method: (a) raw image of letters 'ST' at 19.29 GHz, (b) reconstructed image of letter 'ST' focused on 'S' at 19.29 GHz, (c) raw image of letters 'ST' at 18.56 GHz, and (d) reconstructed image of letter 'ST' focused on 'T' at 18.56 GHz.

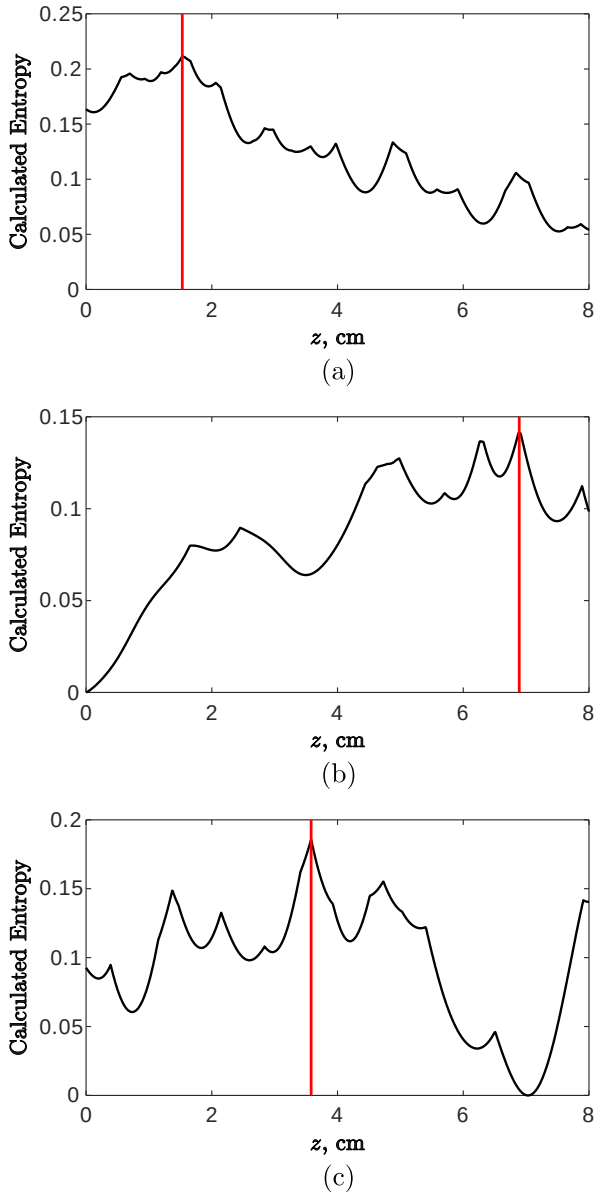

Fig. 8. Calculated entropies according to depth increment: (a) target placed 1.5 cm below, (b) target placed 6.5 cm below, and (c) target placed 3.5 cm below.

V. CONCLUSION

In this paper, an HSR image focusing method was proposed for evaluating images based on an entropy metric. The proposed method iteratively finds the optimal frequency and depth of target objects by assuming the subsurface materials to be free space. For each iteration, the reconstructed image was obtained varying frequency and depth value, and the optimum values were determined through the image evaluation results. The method was validated numerically and experimentally. The numerical validation was used a FDTD based gprMax software package and experimental

validation was used an HSR system configured at a laboratory level. The reconstructed images similarly illustrated the actual shapes of the targets. Thus, the proposed method appears helpful for automated focusing of HSR images.

ACKNOWLEDGMENT

This research was supported by Development of Core Technologies for Advanced Measuring Instruments funded by Korea Research Institute of Standards and Science (KRISS – 2021 – GP2021-0009).

REFERENCES

[1] J. D. Taylor, *Ultrawideband Radar Applications and Design*. CRC Press, Boca Raton, FL, 2012.

[2] J. D. Taylor, *Advanced Ultrawideband Radar Signals, Targets, and Applications*. CRC Press, Boca Raton, FL, 2017.

[3] S. Ivashov, V. Razevig, I. Vasiliev, T. Bechtel, and L. Capineri, "Holographic subsurface radar for diagnostics of cryogenic fuel tank thermal insulation of space vehicles," *NDT & E International*, vol. 69, pp. 48-54, 2015.

[4] S. I. Ivashov, I. A. Vasiliev, T. D. Bechtel, and C. Snapp, "Comparison between impulse and holographic subsurface radar for NDT of space vehicle structural material," *PIERS Online*, vol. 3, no. 5, pp. 658-661, 2007.

[5] A. Zhuravlev, S. Ivashov, I. Vasiliev, and V. Razevig, "Processing of holographic subsurface radar data," in *Proc. 14th Int. Conf. Ground Penetrat. Radar (GPR)*, Shanghai, China, June 4-8, 2012.

[6] J. T. Case, F. L. Hepbum, and R. Zoughi, "Inspection of spray on foam insulation (SOFI) using microwave and millimeter wave synthetic aperture focusing and holography," in *Proc. IEEE Instrum. Meas. Technol. Conf. (I2MTC)*, Sorrento, Italy, Apr. 24-27, 2006.

[7] S. Ivashov, A. Zhuravlev, M. Chizh, and V. Razevig, "High resolution MW holographic system for NDT of dielectric materials and details," in *Proc. 16th Int. Conf. Ground Penetrat. Radar (GPR)*, Hong Kong, June 13-16, 2016.

[8] S. I. Ivashov, V. V. Razevig, I. A. Vasiliev, A. V. Zhuravlev, T. D. Bechtel, and L. Capineri, "Holographic subsurface radar of RASCAN type: Development and applications," *IEEE J. Sel. Topics Appl. Earth Observ. Remote Sens.*, vol. 4, no. 4, pp. 763-778, 2011.

[9] D. M. Sheen, D. L. McMakin, and T. E. Hall, "Three-dimensional millimeter-wave imaging for concealed weapon detection," *IEEE Trans. Microw. Theory Techn.*, vol 49, no. 9, pp. 1581-1592, 2001.

[10] D. Gabor D, "A new microscopic principle," *Nature*, vol. 161, no. 4098, pp. 777-778, 1948.

[11] X. Wei and Y. Zhang, "Autofocusing techniques for GPR data from RC bridge decks," *IEEE J. Sel. Topics Appl. Earth Observ. Remote Sens.*, vol. 7, no. 12, pp. 4860-4868, 2014.

[12] R. L. Morrison, M. N. Do, and D. C. Munson, "SAR image autofocus by sharpness optimization: A theoretical study," *IEEE Trans. Image Process.*, vol. 16, no. 9, pp. 2309-2321, Sep. 2007.

[13] F. Ahmad, M. G. Amin, and G. Mandapati, "Autofocusing of through the-wall radar imagery under unknown wall characteristics," *IEEE Trans. Image Process.*, vol. 16, no. 7, pp. 1785-1795, July 2007.

[14] L. Xi, L. Guosui, and J. Ni, "Autofocusing of ISAR images based on entropy minimization," *IEEE Trans. Aerosp. Electron. Syst.*, vol. 35, no. 4, pp. 1240-1252, Oct. 1999.

[15] S. Podlech S, "Autofocus by Bayes spectral entropy applied to optical microscopy," *Microscopy and Microanalysis*, vol. 22, no. 1, pp. 199-207, 2016.

[16] S. Yazdanfar, K. B. Kenny, K. Tasimi, A. D. Corwin, E. L. Dixon, and R. J. Filkins, "Simple and robust image-based autofocusing for digital microscopy," *Optics Express*, vol. 16, no. 12, pp. 8670-8677, 2008.

[17] C. Warren, A. Giannopoulos, and I. Giannakis, "gprMax: Open source software to simulate electromagnetic wave propagation for ground penetrating padar," *Computer Physics Communications*, vol. 209, pp. 163-170, 2016.

[18] C. Warren, A. Giannopoulos, A. Gray, I. Giannakis, A. Patterson, L. Wetter, and A. Hamrah, "A CUDA-based GPU engine for gprMax: Open source FDTD electromagnetic simulation software," *Computer Physics Communications*, vol. 237, pp. 208-218, 2018.